International Journal Of Engineering Research And Development
e- ISSN: 2278-067X, p-ISSN: 2278-800X, www.ijerd.com
Volume 21, Issue 5 (May 2025), PP 142-151

The Study on the Fracture Evolution of Coplanar two fissured Rock under Uniaxial Compression at Different Moisture Content

Hongrui Liang, Zhongchang Wang, Wenrui Bian, Bohui Shi
(High-speed Railway Technical Engineering Research Center in High-cold Area, Liaoning, Dalian Jiaotong University, Dalian 116028, China)

Abstract*: In order to analyze the influence of fissures on the uniaxial compression failure characteristics of rocks with different moisture contents above and below, a uniaxial compression model of intact rock and fissured rock with different moisture content combinations was constructed using the particle flow software (PFC2D) ,simulating Uniaxial Compression Tests on Water-Bearing Rocks,indentifyingthe moisture content combination resulting in the greatest reduction in peak strength,Furthermore, analyzing the influence of rock fracture inclination angle, fracture length, rock bridge length, and fracture width on the failure characteristics of the rock under the identified moisture content combination . The results indicate that the peak strength is at its lowest when the upper layer moisture content is 15% and the lower layer moisture content is 20%. Under these moisture conditions, the peak strength reaches its minimum when the fracture inclination angle is 90 degrees, the fracture length is 12.5 mm, the fracture width is 2.5 mm, and the rock bridge length is 5 mm, suggesting that fractures have the most severe impact on rock failure under these parameters. Additionally, the highest loss rate of peak strength in water-bearing rocks occurs when the fracture inclination angle is 90 degrees, the fracture length is 5 mm, the fracture width is 0.5 mm, and the rock bridge length is 2.5 mm. Different fracture inclination angles and lengths can alter the failure mode, whereas variations in fracture thickness and rock bridge length do not significantly affect the failure mode. However, cracks in water-bearing rocks tend to propagate in a thicker and longer manner during expansion.*

Key words*：Fractured rock mass; Uniaxial compression; Particle flow; Moisture content; Peak strength*

Date of Submission: 10-05-2025 Date of acceptance: 20-05-2025

I. Introduction

Within the intricate matrix of rock, a myriad of pores and fissures serve as conduits for water in its various forms to infiltrate, leading to the saturation of the rock. Maruvanchery V(2019) discerned that the ingress of water, which diminishes the rock's strength, stands as a pivotal factor contributing to the deformation and failure of rock structures. The presence of water exacerbates the propagation of cracks, leading to further deterioration of the rock structure. Investigating the evolution of fractures in water-bearing rocks is a pressing challenge that demands immediate attention and resolution. At present, research on the evolution of rock fractures is primarily divided into two methodologies: laboratory experiments and numerical simulations. Zida L et al. (2024) conducted uniaxial compression tests on fractured sandstone specimens with varying fracture inclination angles to explore the crack propagation and fracture mechanisms of fractured rock masses. Shi (2020) and G. S, B. V M (2021) took the crack propagation patterns in double-fractured gypsum specimens as a starting point and, based on the crack propagation results from laboratory tests, analyzed the advantages of fracture and large deformation. Cheng et al. (2016) focused on sandstone as their research subject, investigating the mesoscopic cracking evolution and coalescence mechanisms of rock under different normal stress conditions during shearing. Li et al. (2021) utilized pyroxene syenite as their material and conducted uniaxial compression experiments using a rock mechanics servo testing machine to analyze the laws of crack initiation, propagation, and coalescence failure in rocks with varying numbers of fractures. Li et al. (2024) performed uniaxial compression tests on pre-fabricated sandstone specimens with unequal-length fractures to study the influence of different fracture lengths on rock failure under uniaxial compression. Haeri H et al. (2014) conducted compression loading tests on cylindrical specimens of rock-like materials containing pre-existing cracks, observing the initiation and coalescence stresses during the crack propagation process. Compared to laboratory experimental methods, numerical simulation approaches are more readily implementable, entail lower experimental costs, and are subject to smaller margins of error. Zhou et al. (2024)used the FLAC3D program to simulate the deformation and failure patterns of fractured rock masses with varying inclination angles, apertures, and numbers of fractures under uniaxial compression conditions. Zhang et al. (2025) utilized the Grain-Based Model (GBM) method to model the microscopic mineral composition of sandstone, investigating the effects of mineral content, mineral grain size, and the heterogeneity of mineral grain size distribution on compressive strength. Park I et al. (2003) employed numerical analysis methods to study mixed-mode crack propagation in rocks. Feng et al. (2022), Liu et al. (2022), and Wang (2023) conducted research based on PFC2D to study the crack propagation patterns and shear characteristics of rocks containing intersecting fractures under direct shear conditions, as well as the crack propagation in composite rock samples, revealing the mechanical properties and response laws of deep fractured rocks. Therefore, this paper employs the PFC2D particle flow software to investigate the failure characteristics of pre-existing coplanar double-fractured rock specimens under uniaxial compression with varying moisture content conditions above and below. The aim is to identify the combination of upper and lower moisture contents that most severely affects rock failure. Furthermore, under this moisture content condition, the study explores the influence of different fracture inclination angles, fracture lengths, fracture widths, and rock bridge lengths on the degree and mode of rock failure.

II. Establishment Of Numerical Models And Simulation Schemes

2.1 The establishment of the numerical model involves

In Particle Flow Code (PFC), various contact models are available, including linear, contact bond, and parallel bond models. Among these, the parallel bond model is particularly effective in capturing the mechanical behavior of geomaterials, such as rocks and soils. Therefore, in this study, the parallel bond model is selected for the contacts between particles to accurately simulate the mechanical response of the rock specimens.The numerical specimen has a height H of 100mm and a width W of 50mm, with a total of 12,219 particles generated. The rock is divided into two parts along the midline of its height, each assigned a different moisture content. Particles are removed on both sides of the contact surface to create a fracture. As illustrated in Figure 1, the compression test employs displacement loading. Opposite but equal in magnitude velocities (0.1 m/s) are applied to the top and bottom walls of the specimen to achieve unconfined uniaxial compression loading of the specimen. During the loading process, a Fish program is utilized to document the stress-strain response of the specimen and the generation of microcracks throughout the loading phase. The numerical test is terminated when the post-peak strength declines to 70% of the peak strength. Figure 2 presents the geometric parameters of the numerical model for the fractured rock.

Fig. 1 Numerical Sample Model **Fig. 2**Geometrical Parameter

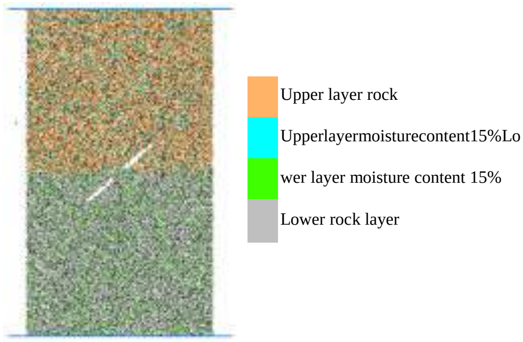

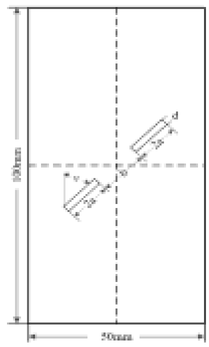

Before conducting numerical simulations, it is essential to first calibrate the mesoscopic parameters. In the parallel bond model, it primarily encompasses mesoscopic parameters such as the friction coefficient, contact modulus, stiffness ratio, and bond strength. Calibration is achieved by continuously adjusting the mesoscopic parameters until the simulation results closely match the experimental outcomes (Wang et al. 2024) . Through iterative adjustments, a set of mesoscopic parameters that accurately reflect the macroscopic mechanical properties of sandstone and rock-soil was ultimately obtained. The stress-strain curves, strength and elastic modulus, crack propagation process, and failure modes simulated using these mesoscopic parameters all closely align with the results from laboratory tests. Table 1 presents the mesoscopic parameters for the particle flow simulation of sandstone employed in this study.

Tab. 1 The mesoscopic parameters for the particle flow simulation of sandstone are as follows

Parameter of particle	**Values**	**Parameter of particle**	**Values**
Minimum particle radius/mm	0.24	Particle friction coefficient	0.5
Particle size ratio	1.5	Parallel bond modulus/GPa	40
Particle density/(kg·m^{-3})	2700	Parallel bond stiffness ratio	2.5
Particle contact modulus/GPa	40	Mean normal bond strength/MPa	50
Particle stiffness ratio	2.5	Mean tangential bond strength/MPa	50
Water particle density/(kg·m^{-3})	1000	Water particle stiffness ratio	0.5

2.2 The failure process of fractured rock under uniaxial compression conditions (taking a fracture inclination angle of 45° and a water content of 15% as an example)

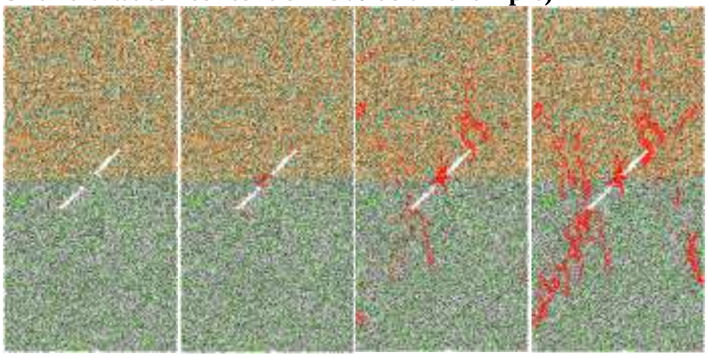

Fig. 3 Numerical Specimen and Geometric Parameters of Fractured Rock Mass

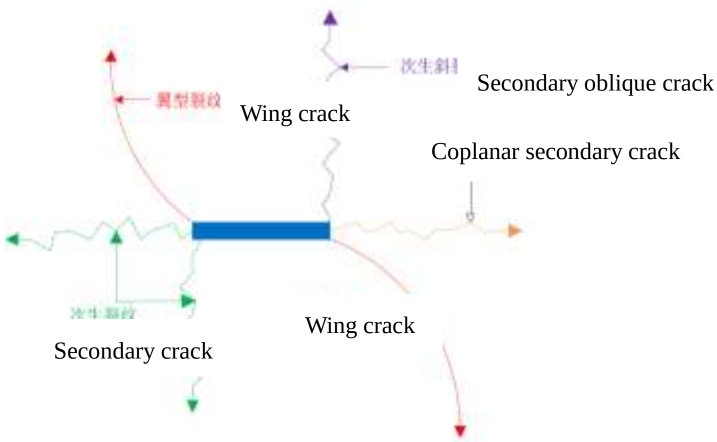

Fig. 4 Crack Propagation Modes Under Uniaxial Compression

Figure 3 illustrates the failure process of fractured rock with a fracture inclination angle of 45° and a water content of 15% in both the upper and lower sections. From the figure, it can be observed that crack propagation generally produces three types of cracks, as shown in Figure 4: wing cracks (tensile cracks), coplanar secondary cracks (shear cracks), and oblique secondary cracks (shear cracks).During the loading process, wing cracks first appear at the tips of the fractures, exhibiting a tensile failure mode (Mode I fracture propagation). Subsequently, coplanar secondary cracks and oblique secondary cracks emerge, displaying a shear failure mode (Mode II fracture propagation). As loading continues, the propagation direction of the wing cracks gradually aligns with the loading direction, and the width of the secondary cracks increases continuously. The initiation, propagation, and coalescence of multiple cracks within the specimen lead to the final instability and failure of the numerical specimen, manifesting as a macroscopic tensile-shear composite failure mode (Mode I-II mixed failure).The connection of the two fractures is achieved through the propagation and coalescence of coplanar secondary cracks originating from the right tip of the left fracture and the left tip of the right fracture.

2.3 Numeric simulation scheme

Numerical simulation is divided into two stages.

The first stage is the water content simulation stage, where the crack length 2a=10mm, crack width d=1mm, rock bridge length b=5mm, crack inclination angle α=90 ° are set, and the crack is placed on the contact surface. Set different moisture contents in the upper and lower layers of the rock mass, ranging from 0% to 30%, and conduct numerical simulations in sequence to obtain the combination of upper and lower moisture contents with the highest strength loss rate.

The second stage is the crack simulation stage. Based on obtaining the combination of moisture content with the highest strength loss rate, the crack inclination angle, crack length, crack width, and rock bridge length are modified to further explore the peak strength loss under different crack conditions. The specific plan is as follows:
(1) Crack width d=1mm, crack length 2a=10mm, rock bridge length b=5mm, crack inclination angles α=0 °, 15 °, 30 °, 45 °, 60 °, 75 °, 90 °.
(2) Crack width d=1mm, crack inclination angle α=45 °, rock bridge length b=5mm, crack length 2a=2.5, 5, 7.5,

10, 12.5mm
(3) Fracture length 2a=10mm, rock bridge length b=5mm, fracture inclination angle α=45 °, fracture width d=0.5, 1.0, 1.5, 2.0, 2.5mm
(4) Crack width d=1mm, crack length 2a=10mm, crack inclination angle α=45 °, rock bridge length b=2.5, 5, 7.5, 10, 12.5mm

III. Simulation Analysis Of Macroscopic Failure Characteristics Of Fractured Rocks Under Different Moisture Contents

3.1 Analysis of moisture content results

The moisture content of sandstone is set to 0%, 5%, 10%, 15%, 20%, 25% and 30% respectively, and then under the above seven conditions, each moisture content is set below to set 0%, 5%, 10%, 15%, 20%, 25% and 30% to obtain the rock failure and peak strength of different water content combinations, and the water content combination of 15% above and below is taken as an example, and the simulation results are verified by comparing with the experimental data, as shown in Figure 5. The peak intensity of each combined stress is recorded, and the results are shown in Table 2.

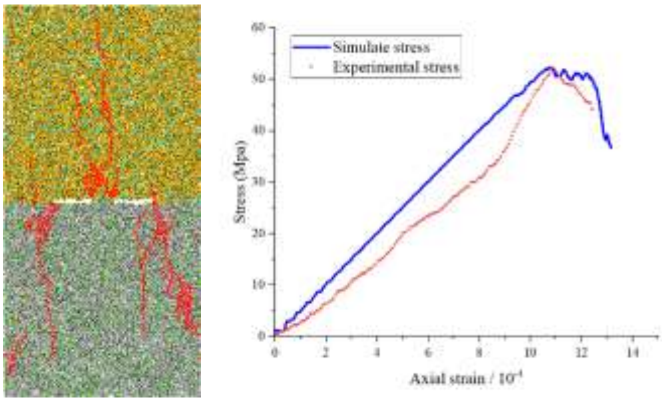

Fig. 5 Numerical simulation results and peak strength with both upper and lower moisture contents of 15%

Tab. 2 Peak intensity of different combinations of moisture content

Upper / below	0%	5%	10%	15%	20%	25%	30%
0%	57.8Mpa	56.1Mpa	54.1Mpa	53Mpa	42.2Mpa	46.6Mpa	57.3Mpa
5%	55.2Mpa	51.2Mpa	54.2Mpa	51Mpa	57Mpa	47.2Mpa	54.9Mpa
10%	53.8Mpa	53.2Mpa	45.6Mpa	49.5Mpa	50.4Mpa	47.2Mpa	54.2Mpa
15%	51.2Mpa	48.8Mpa	48.3Mpa	51.9Mpa	41.9Mpa	50.2Mpa	45.2Mpa
20%	55.4Mpa	45.9Mpa	48.2Mpa	48.1Mpa	50Mpa	52.3Mpa	50.4Mpa
25%	46.1Mpa	51Mpa	46.8Mpa	45.1Mpa	50.7Mpa	50.2Mpa	47.4Mpa
30%	50.5Mpa	42Mpa	53.5Mpa	43Mpa	49.9Mpa	49.2Mpa	55.2Mpa

According to the results in Table 2, it can be seen that the peak strength of rocks with different water content combinations has decreased compared to intact rocks with 0% upper and lower water content, indicating that combinations with different water content will cause varying degrees of damage to rocks. In order to more intuitively reflect the peak intensity of each moisture content combination, the data is plotted as a contour map filled with colors, as shown in Figure 6. It can be intuitively observed that the combination with a moisture content of 15% above and 20% below has the highest peak loss, and this combination has the most severe damage to the rock due to moisture content. Next, based on this combination of moisture content, we will simulate the effects of different fracture angles, fracture lengths, fracture thicknesses, and rock bridge lengths on rock failure.

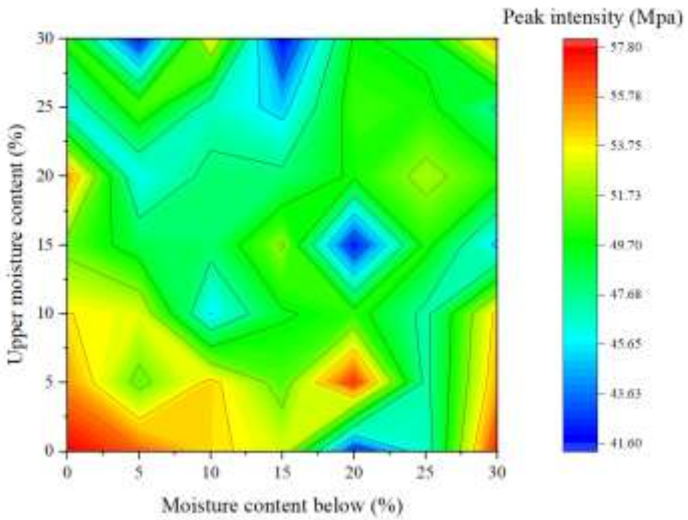

Fig. 6 Peak strength of rocks with different combinations of moisture content

3.2 Fracture inclination angle

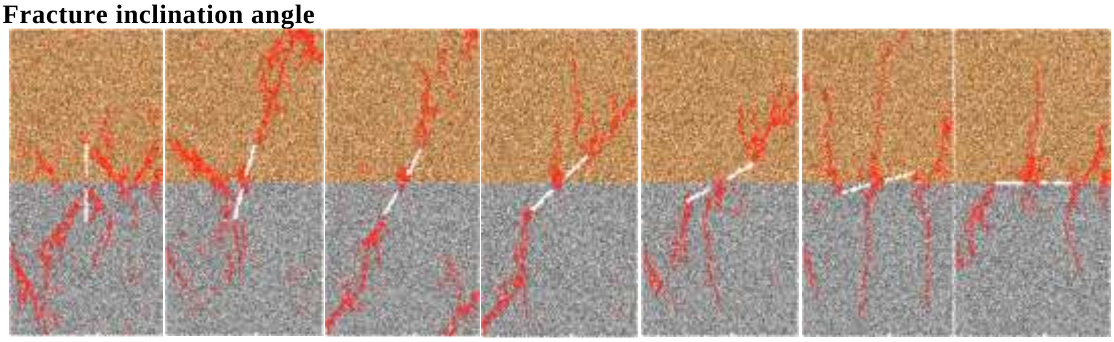

α=0° α=15° α=30° α=45° α=60° α=75° α=90°

(No water bearing rocks)

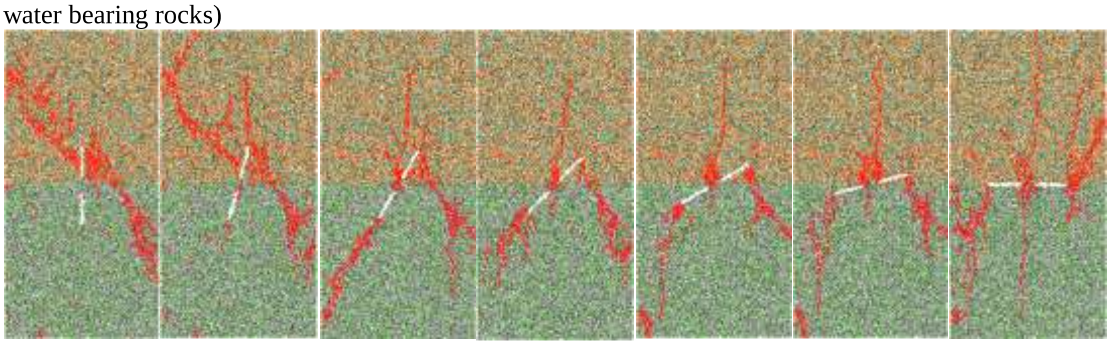

α=0°α=15°α=30°α=45°α=60°α=75° α=90°

(Waterbearing rocks)

Fig. 7 Whether the failure characteristics of water bearing rocks under different fracture angles

Figure 7 shows the rock failure characteristics with different fracture angles and water content. According to Figure 13, it can be seen that in no water bearing rocks, when the fracture angle is 0 ° and the fracture angle is 15 °, the final failure surface overlaps with a fracture, exhibiting a macroscopic shear failure mode. When the inclination angle is 30 °, it exhibits a macroscopic shear failure mode, where the failure surface and two cracks overlap. When the inclination angle is 45 °, 60 °, and 75 °, it mainly exhibits a macroscopic tension shear composite failure mode. As the inclination angle increases, secondary cracks gradually become thinner, and cracks generated by rock bridge penetration are promoted and expand outward, reaching the outside of the rock at 75 °. However, this trend weakens at 90 °.

When water is present, macroscopic shear failure occurs at inclination angles of 0 ° and 15 °, and at 15 °, the final failure surface overlaps with a crack. When the inclination angles are 30 °, 45 °, 60 °, 75 °, and 90 °, many macroscopic tension type cracks appear during rock failure, mainly manifested as a macroscopic tension shear composite failure mode. As the angle increases, the secondary cracks gradually become thinner, but compared to rocks without water at the same inclination angle, the secondary cracks are coarser. The cracks at the rock bridge are promoted and gradually propagate outward as macroscopic tensile cracks, reaching the outside of the rock at α=90 °.

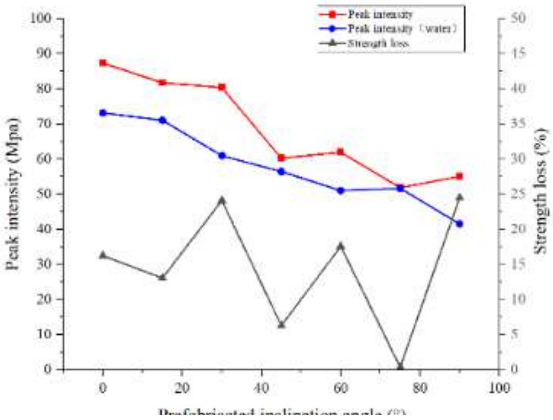

Fig. 8 Whether the peak strength changes of water bearing rocks under different fracture angles

Figure 8 shows the variation of rock strength at different fracture angles before and after freeze-thaw cycles. As shown in Figure 8, with the increase of fracture inclination angle, the peak strength of no water rock will decrease, but there will be a slight rebound at 60 ° and 90 °, while the peak strength of rock with 15% water above and 20% water below will generally show a monotonic decreasing trend. The minimum value of peak strength without water occurs at a rock fracture dip angle of 75 °, with a value of 51.9MPa, while the minimum value of peak strength with water is 41.6MPa, occurring at a rock dip angle of 90 °, with a rock strength loss rate of 24.6%. Overall, the influence of fracture angle on rock strength is complex, and water can lead to a decrease in rock strength.

3.3 crack length

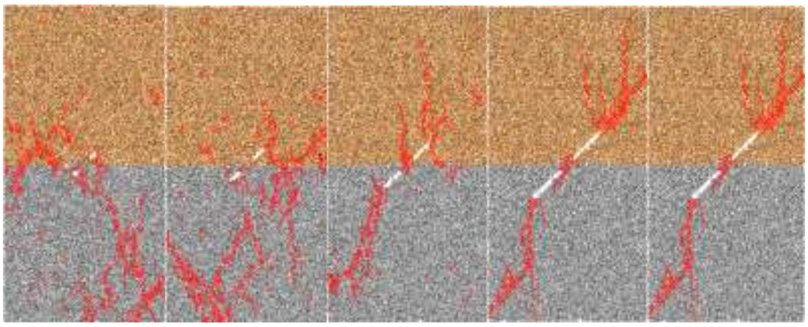

2a=2.5 2a=5 2a=7.5 2a=10 2a=12.5

(No water bearing rocks)

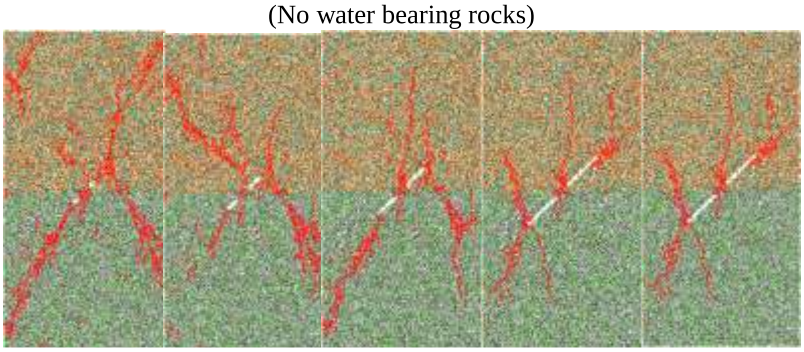

2a=2.5 2a=5 2a=7.5 2a=10 2a=12.5

(Waterbearing rocks)

Fig. 9 Whether the failure characteristics of water bearing rocks under different crack lengths

Figure 9 shows the failure characteristics of rocks with different crack lengths and water content. When there is no water content, the crack length is 2.5mm and 5mm, and the crack is not connected to the damage, and the rock bridge is not connected. The crack length is 7.5-12.5mm, mainly exhibiting a macroscopic tension shear composite failure mode. At 7.5mm, the rock bridge penetrates and expands as a macroscopic tension type crack, but at 10mm and 12.5mm, although the rock bridge penetrates, it does not continue to expand. The secondary crack propagation on both sides of the 10mm and 12.5mm cracks is more pronounced compared to 7.5mm cracks, but there is no significant difference between 10mm and 12.5mm cracks.

Compared to not containing water, when containing water and the crack length is 2.5mm, it exhibits macroscopic shear failure, which is connected to two cracks and connected by a rock bridge. When the crack length is 5mm, the failure mode is somewhat similar to that of 2.5mm. There are fewer secondary cracks on both sides compared to 2.5mm, but shear failure occurs after the rock bridge is penetrated. When the crack length is 7.5mm, the failure mode is similar to that without water, but the secondary cracks on both sides and the tensile cracks after the rock bridge is connected propagate thicker and longer. 10mm and 12.5mm are basically the same, but compared to the absence of water, they exhibit a macroscopic tension shear composite failure mode, with secondary cracks on both sides becoming thinner but increasing, and continuing to propagate after the rock bridge is penetrated.

Figure 10 shows the changes in peak strength and failure characteristics of rocks with different crack lengths before and after freeze-thaw cycles. The peak strength of rocks before and after freeze-thaw decreases with the increase of crack length. When the length of prefabricated cracks increases from 2.5mm to 12.5mm, the peak strength of unfrozen rocks decreases by 40.6%, and the peak strength of rocks with water content decreases by 32.3%. This indicates that the increase in crack length will reduce the peak strength of rocks, and the impact on water containing rocks is significantly greater than that on no water containing rocks. Comparing the strength loss rates of rocks with different fracture lengths before and after freeze-thaw, it can be seen that as the fracture length increases, the overall strength loss rate of water bearing rocks gradually fluctuates and decreases, with values of 16.3%, 16.6%, 10.7%, 4.5%, and 4.9%, respectively. So when the crack length is 5mm, water content causes the most severe damage to the rock.

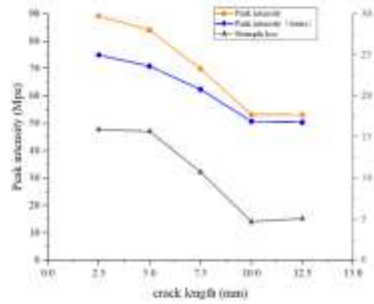

Fig. 10 Whether the peak strength varies under different fracture dip angles in water-bearing rocks

3.4 Crack width

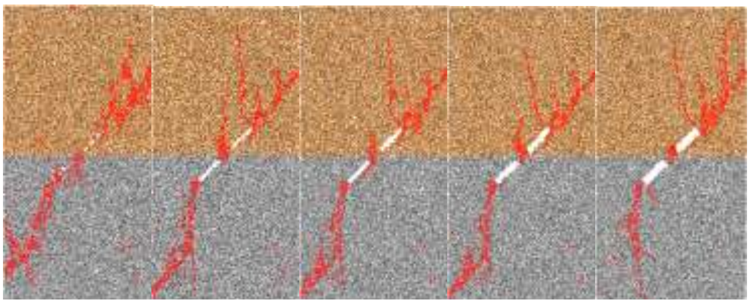

d=0.5 d=1 d=1.5 d=2 d=2.5

(No water bearing rocks)

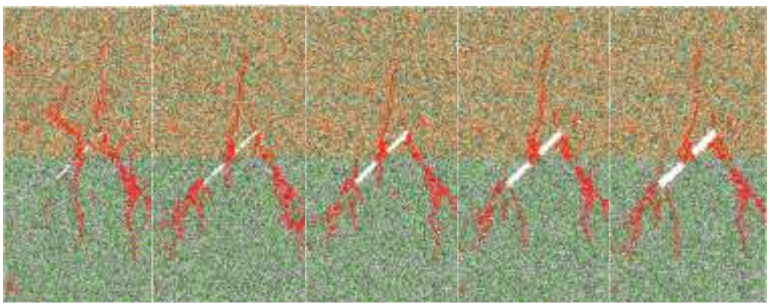

d=0.5 d=1 d=1.5 d=2 d=2.5

(Waterbearing rocks)

Fig. 11 Whether the failure of water-bearing rocks occurs under conditions of varying fracture widths

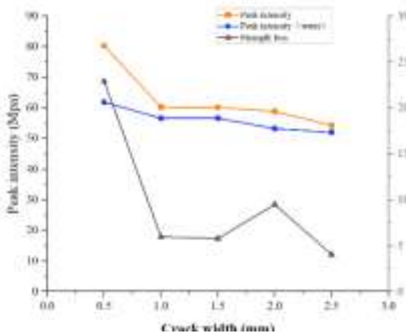

Fig. 12 Whether the peak strength of water-bearing rocks varies under conditions of different fracture widths

Figures 11 and 12 illustrate the variation patterns of peak strength and failure characteristics of rocks with different fracture widths under both dry and water-bearing conditions. It can be observed that the fracture width does not significantly influence the failure mode of the rocks. Under dry conditions, the failure mode is primarily characterized by macroscopic shear failure. When the fracture width exceeds 1 mm, wing cracks do not continue to propagate, and secondary cracks show no significant change between 1–2 mm but decrease at 2.5 mm. Although rock bridges are connected, shear failure does not continue to occur at 2.5 mm. Under water-bearing conditions, the failure mode is mainly a combination of tensile-shear failure. At 1 mm, the propagation of secondary cracks on both sides is more pronounced compared to 0.5 mm, and tensile failure is also more extensive after the rock bridges are connected. However, beyond 1 mm, the degree and mode of failure show no significant changes. As shown in Figure 12, the peak strength decreases significantly before 1 mm but remains relatively unchanged thereafter. The strength loss rate is highest at a fracture width of 0.5 mm, reaching 22.8%. Therefore, under water-bearing conditions, rock failure is most severe when the fracture width is 0.5 mm.

3.5 Rock Bridge Length

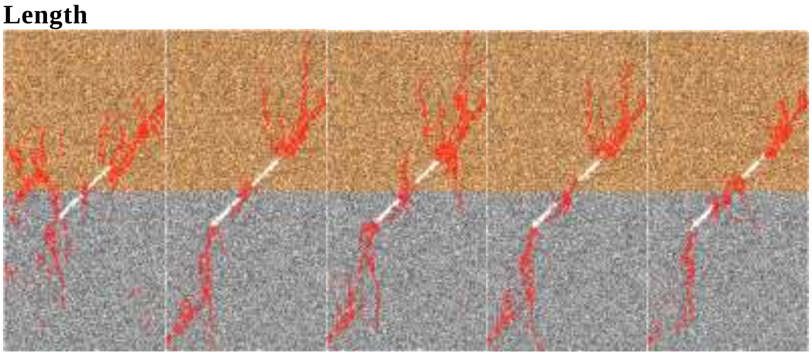

b=2.5 b=5 b=7.5 b=10 b=12.5

(No water bearing rocks)

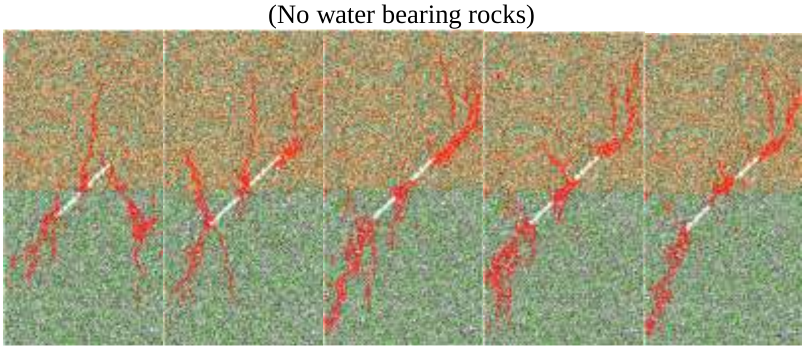

b=2.5 b=5 b=7.5 b=10 b=12.5

(Waterbearing rocks)

Fig. 13 Whether the failure of water-bearing rocks occurs under conditions of varying rock bridge lengths

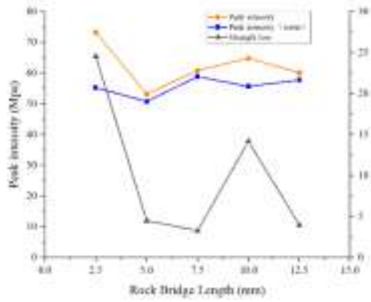

Fig. 13 Whether the peak strength of water-bearing rocks varies under conditions of different rock bridge lengths

Figures 13 and 14 depict the variation patterns of peak strength and failure characteristics of rocks with different rock bridge lengths under both dry and water-bearing conditions. The length of the rock bridge does not significantly affect the failure mode. For dry rocks, the primary failure mode is shear failure. The rock bridges are connected, but the cracks in the rock bridges do not propagate further. Secondary cracks increase at 10 mm but then gradually decrease. The peak strength generally exhibits an "inverted N" shape, showing a significant decline between 2.5 and 5 mm, a slow recovery between 5 and 10 mm, and a gradual decrease between 10 and 12.5 mm. Under water-bearing conditions, the failure mode is primarily a combination of tensile-shear failure. After the rock bridges are connected, the tensile cracks generated in the rock bridges gradually shorten, and the secondary cracks on both sides gradually decrease but become thicker and longer. The peak strength variation generally follows a "W" shape, with slow decreases between 2.5–5 mm and 7.5–10 mm, and slow increases under other conditions. The peak strength drops sharply between 2.5 and 5 mm, stabilizes between 5 and 12.5 mm, but shows a slight recovery fluctuation at 10 mm. Overall, the peak strength loss is highest at a rock bridge length of 2.5 mm, reaching 24.5%. Therefore, the rock is most severely damaged when the rock bridge length is 2.5 mm.

IV. Conclusion

This study investigates the mesoscopic damage mechanisms of fractured rocks with varying water contents based on physical experiments and PFC2D discrete element numerical simulations. It also discusses the energy evolution and failure characteristics of fractured rocks with different water contents in the upper and lower layers. Furthermore, it analyzes the influence of fracture parameters on the peak strength of rocks under both dry and water-bearing conditions. The main conclusions are summarized in the following five points:

(1) The presence of water deteriorates the physical properties of rocks. Compared to dry rocks, the peak strength of water-bearing rocks decreases under various fracture parameters. The highest strength loss rate occurs when the upper layer has a water content of 15% and the lower layer has a water content of 20%.

(2)As the dip angle increases, the failure mode of both dry and water-bearing rocks transitions from macroscopic shear failure to macroscopic tensile-shear failure. Water content does not affect the failure mode, but crack propagation is more extensive in water-bearing rocks. Dry rocks experience the highest strength loss at a dip angle of 75°, while water-bearing rocks experience the highest strength loss at a dip angle of 90°. The influence of water on rock strength is most significant at a dip angle of 90°.

(3)The fracture length has little influence on the failure mode of rocks. Dry rocks primarily exhibit macroscopic shear failure, while water-bearing rocks mainly show macroscopic tensile-shear failure. Compared to dry rocks, crack propagation in water-bearing rocks is more pronounced after the rock bridges are connected. The minimum peak strength for both occurs at a fracture length of 12.5 mm, but the maximum strength loss rate occurs at a fracture length of 5 mm.

(4) The fracture thickness generally does not affect the failure mode of rocks and has little influence on strength loss. After the fracture thickness exceeds 1 mm, the peak strength stabilizes but continues to decrease slightly. The minimum peak strength for both dry and water-bearing rocks occurs at a fracture thickness of 2.5 mm. The fracture thickness with the greatest influence of water on rock strength is 0.5 mm, where the peak strength loss rate is the highest.

(5) Under different rock bridge lengths, dry rocks primarily exhibit macroscopic shear failure, while water-bearing rocks mainly show macroscopic tensile-shear failure. As the rock bridge length increases, the cracks generated after the rock bridges are connected gradually shorten. However, water-bearing rocks develop more secondary cracks on both sides. The minimum peak strength for both occurs at a rock bridge length of 5 mm, while the highest strength loss rate occurs at a rock bridge length of 2.5 mm, where water-induced damage to the rock is most severe.

REFERENCE

[1]. Maruvanchery V ,Kim E (2019) Effects of water on rock fracture properties: Studies of mode I fracture toughness, crack propagation velocity, and consumed energy in calcite-cemented sandstone, Geomechanics and Engineering,17(1):57-67.

[2]. Zida L, Diyuan L, Jianqiang X, et al. (2024) Quantitative investigation of crack propagation and fracture mechanism of fissured sandstone from the mesoscopic perspective, Theoretical and Applied Fracture Mechanics,129

[3]. Shi Y(2020)Research on the mechanism of double crack propagation in rock like materials based on discrete element numerical method, Chengdu: South China University of Technology.**(in Chinese)**

[4]. G. S,B. V M (2021)Crack growth in rocks with preexisting narrow flaws under uniaxial compression , International Journal of Geomechanics,21(4)

[5]. Cheng L Z, Xu J, Feng D, et al.(2016) The Influence of Normal Stress on the Evolution and Propagation mechanism of rock shear cracks, Journal of Mining and Safety Engineering,33(04):741-746+753**(in Chinese)**

[6]. Li G Q,Ma H C,Qian J Z,et al. (2021) Rock fracture tests and simulations with different numbers of cracks,Industrial Construction,51(09):181-187**(in Chinese)**

[7]. Li Q, Kang J, Li S B,et al. (2024) The influence of geometric parameters of unequal length cracks on the strength and crack propagation of sandstone, Mining Research and Development,44(10):141-149**(in Chinese)**

[8]. Li Z Y, Gao S, Shen S Q, et al.(2025) Experimental study on the influence of water immersion time on the strength and failure characteristics of rock mass, Chinese Journal of Rock Mechanics and Engineering,44(01):99-113.**(in Chinese)**

[9]. Haeri H,Shahriar K,Marji F M, et al. (2014) Onthestrengthandcrackpropagationprocessofthepre-crackedrock-likespecimensunderuniaxialcompression, Strength of Materials,2014,46(1):140-152

[10]. Zhou L, Li Y, Liao C L, et al. (2024) Study on the influence of fracture geometry characteristics on rock mechanical properties under uniaxial compression conditions, Mining Technology,2024,24(01):30-35**(in Chinese)**

[11]. Zhang Q H,Ma R Y, Lin P, et al. (2025) The influence of mineral composition on the uniaxial compression mechanical properties of sandstone based on PFC-GBM method, Journal of Shandong University (Engineering Science),1-18**(in Chinese)**

[12]. Park I,Lee C(2003) Mixed mode crack propagation in rock using numerical analysis, International Journal of Rock Mechanics and Mining Sciences,2003,41(3):359-359.

[13]. Feng H T,Chen J Z,Ren C F(2022)Numerical study on crack propagation and shear characteristics of fractured rocks,Journal of Safety Science and Technology,18(06):134-140**(in Chinese)**

[14]. Liu Y L(2022)Research on the uniaxial compression mechanical characteristics and discrete element numerical simulation of composite rock mass,Fujian Building Materials,(04):7-10+14**(in Chinese)**

[15]. Wang C H (2023)Research on the Damage Evolution Mechanism of Fractured Rock Mass under Dynamic Load Based on PFC, Hengyang:University of South China**(in Chinese)**

[16]. Wang Z M,Yang J J,Wu Y L (2024)Overview of Physical and Chemical Properties of Sandstone Waste at Home and Abroad,Stone,(01):148-149+155**(in Chinese)**